Crustal Fault Zones: New targets for geothermal exploration? Insights from the Pontgibaud Fault Zone in the French Massif Central

Hugo Duwiquet, Laurent Guillou-Frottier, Mathieu Bellanger, Laurent Arbaret, Michael Heap

Proceedings World Geothermal Congress 2020
Reykjavik, Iceland, April 26 – May 2, 2020

Crustal Fault Zones: New targets for geothermal exploration? Insights from the Pontgibaud Fault Zone in the French Massif Central.

Hugo Duwiquet*[1,2,3], Laurent Guillou-Frottier[1,2], Mathieu Bellanger[3], Laurent Arbaret[1] and Michael J. Heap[4]

[1] ISTO, UMR 7327, Université d'Orléans, CNRS, BRGM, 1A rue de la Férollerie, 45071, Orléans, France

[2] BRGM, 3 av. C. Guillemin, BP39009, 45060, Orléans, Cedex 2, France

[3] TLS-Geothermics, 92 Chemin de Gabardie, 31200, Toulouse, France

[4]Institut de Physique de Globe de Strasbourg, UMR 7516 CNRS, Université de Strasbourg/EOST, 5 rue René Descartes, 67084, Strasbourg cedex, France

*hugo.duwiquet@gmail.com

Keywords: Permeability, connected porosity, numerical modelling, high-temperature geothermal system, Pontgibaud Fault Zone, French Massif Central.

ABSTRACT

Using a multidisciplinary approach, the present study aims to understand the potential of a new and novel type of geothermal system for high temperature and electricity production: Crustal Fault Zones (CFZ). Due to an intensive multivariate dataset, the Pontgibaud fault zone emerges as an ideal case study for understanding the factors controlling fluid flow in a fault zone system. 2D and 3D numerical modelling, as well as field and laboratory data, made it possible to quantify this new geothermal resource.

1. INTRODUCTION

Crustal Fault Zones (CFZ) can be defined as crustal-scale heterogeneities, which localize the deformation and thus modify the mechanical properties of the crust, down to Brittle-Ductile Transition (BDT), whose depth depends on the local thermo-mechanical regime. In some cases, CFZ may cross the BDT or even extend below it (e.g. Famin et al., 2004; Jolivet et al., 2004). Thus, CFZ could represent efficient conduits for fluid flow up to temperatures that can exceed 400 °C (Violay et al., 2017)

These CFZ can be found worldwide and their geothermal potential can be highlighted by the occurrence of geothermal events, such as the North Anatolian Fault Zone in Turkey (Süer et al., 2008), the Liquine-Ofqui fault zone in Chile (Lahsen et al., 2010), or the Badenweiler-Lenzkirch Sutur in Germany (Brockamp et al., 2015). However, their geothermal potential has never been studied or quantified.

One such example, the Pontgibaud fault zone (PFZ, French Massif Central), is a 30 km-long and 3.5 km-wide mineralized fault zone. The PFZ is also characterized by numerous CO_2-rich-thermo-mineral springs. Moreover, this area is also defined by a local and regional surface heat flow value of 110 $mW.m^{-2}$ (International Heat Flow Commission database) and temperature gradients between 37 and 41 °C/km. The PFZ has been well studied in the last few years (Bellanger et al., 2017, Ars et al., 2019, Duwiquet et al., 2019). The present study aims at investigating the possibility that the PFZ hosts an active hydrothermal system.

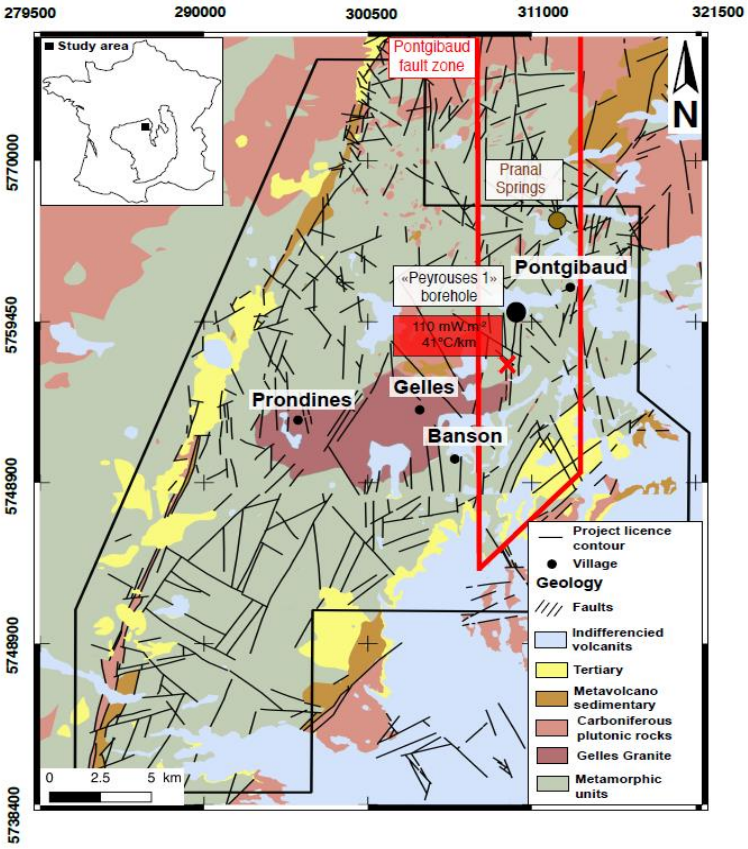

Figure 1 : Simplified geological map showing the "La Sioule" licence area and a brief overview of the major units in the study area. The Pontgibaud Fault Zone is shown in red line. Location of Pranal springs (brown dot). Drilling of "Peyrouses 1" (black dot) Heat flow and geothermal gradient (red crosses, International Heat Flow Commission)

2. FIELD OBSERVATIONS

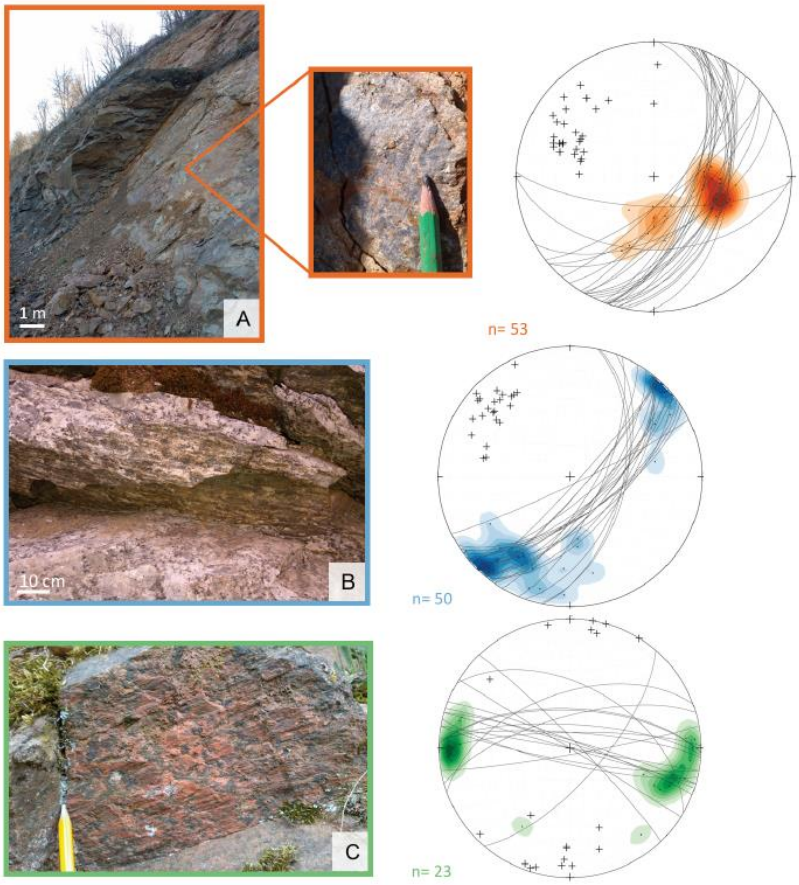

Figure 2 : Observations of the different lithologies and fault families present in the Pontigbaud fault zone. [A] and [C] Metamorphic series. [B] Gelles granite. Schmidt's projection on the lower hemisphere [A], [B], [C].

This approach aims to characterize the deformation as well as the general geometry of the Pontgibaud fault zone. These observations are key to improve the geometry and scaling of the 2D and 3D numerical model. Both observations and geometrical features have been used in our numerical simulations, presented below.

A field study was focused on the Pontgibaud fault zone. More than 120 dip and kinematic measurements were made. Three fault families belonging to the Pontgibaud fault zone can be identified.

The first family is observed on the metamorphic series and comprises 67° ESE dipping normal N 10° trending vein beam faults (Fig 2A).

The second family is formed of mainly dextral N 30° trending faults and are observed on the Gelles granite (Fig 2B).

The third family is observed on the metamorphic series and consists of sinistral faults that trend N°115 (Fig 2C).

These initial observations therefore show that the Pontgibaud fault zone is very fractured and altered. At the scale of the Pontgibaud fault zone, permeability will therefore be very heterogeneous.

3. LABORATORY OBSERVATIONS AND MEASUREMENTS

3.1 Qualitative approach: thin-section and X-ray micro-tomography observations

In order to qualitatively and quantitatively characterize the permeability and porosity parameters of the hydrothermal zone, 2D thin-section observations, 3D X-ray micro-tomography observations and laboratory measurements of permeability and connected porosity were performed. The microstructural analysis of the samples collected within this hydrothermal zone ("Peyrouses 1" borehole, Fig 1) will provide an understanding of how fluids flow within this deformed zone.

Thin-section observations show fracture-rich and highly altered facies. These fractures are mainly filled with quartz, feldspar, phyllosilicates and oxide minerals. Fluid circulation within the fracture seems to promote the crystallization of secondary mineral phases, such as quartz (Fig 3B). Fluid circulation seems to be favored through fractures. However, this circulation can only occur if the fractures are connected to each other. Three-dimensional imaging is therefore required to qualitatively estimate the connectivity of these microstructural elements.

.

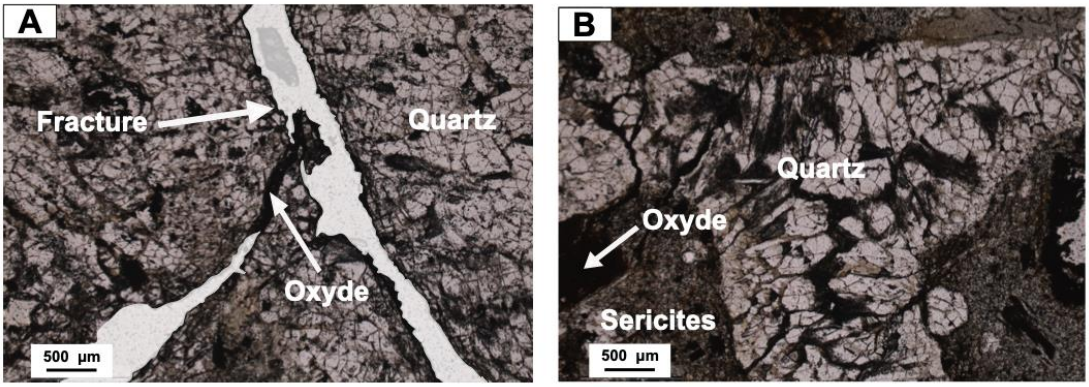

Figure 3 : Microscopic observations of thin-sections from the hydrothermal zone (sample "19-2-1", taken from the "Peyrouses 1" borehole).

X-ray micro-tomography is a non-destructive imaging technique that provides a 3D visualization of the analyzed samples. This imaging technique makes it possible to obtain a voxel resolution between 25 and 4 μm. The 3D volume analysis and processing was performed using the Volume Graphics VG Studio Max software (https://www.volumegraphics.com/en/products/vgstudio-max.html)

On the "19-2-1" sample, we observed the 3D microstructure distribution. The results of the reconstruction and image processing are shown in Fig 4. Figure 4 shows the full sample with a voxel resolution of 25 μm. This sample is characterized by a matrix (grey in Fig 4), fractures (yellow in Fig 4), and mineralizations (red in fig 4). The 3D visualization shows a high density of fractures. These fractures are distributed heterogeneously in space. The apparent connectivity between fractures seems to promote fluid circulation.

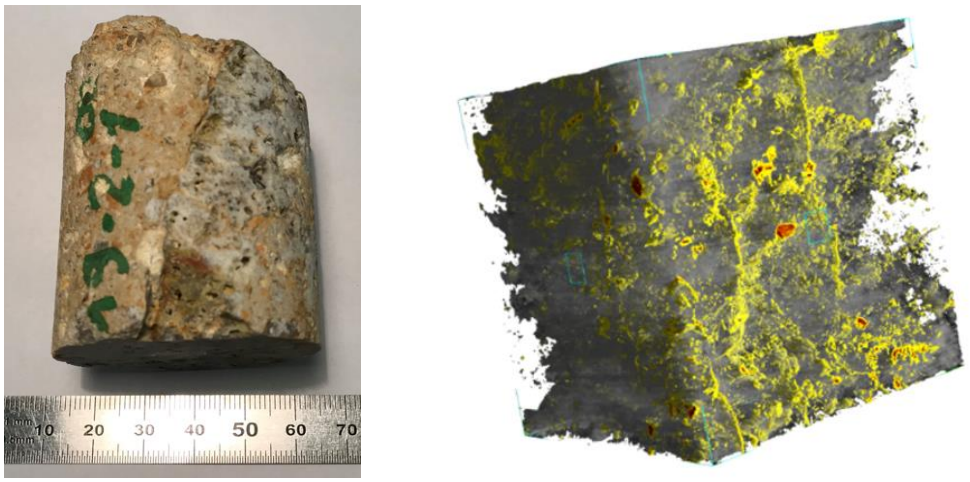

Figure 4 : Three-dimensional observations of the planar porosity on "19-2-1" sample. The yellow colour of figure corresponds to the planar porosity. Red color corresponds to mineralization (lead sulphides). The resolution of figures is 25 μm.

Coupling 2D (thin section) and 3D (micro-tomography) approaches highlights both the system's heterogeneity and the ability of the fluid to circulate through fractures. Because this small-scale porous network can play a crucial role in fluid circulation within the Pontgibaud hydrothermal zone, we also performed direct measurements of connected porosity and permeability.

3.2 Quantitative approach: porosity and permeability measurements

The porosity and permeability of select samples were measured on the equipment available at the École et Observatoire des Sciences des Sciences de la Terre (EOST) in Strasbourg. Measurements were performed on the same samples for which the porosity was visualized using X-ray micro-tomography and thin section analysis (including intact samples, fractured samples, altered samples, and finally, altered and fractured samples). The followed experimental procedure is the one described by Heap & Kennedy (2016).

These measurements were performed on the seven samples for which the porosity was visualized by X-ray micro-tomography. The permeability values vary between 2×10^{-18} and 7×10^{-13} m^2, while the connected porosity values vary between 6 and 22 % (Fig 5). Overall, permeability increases as a function of increasing connected porosity, as illustrated by the two extreme values in Fig 5.

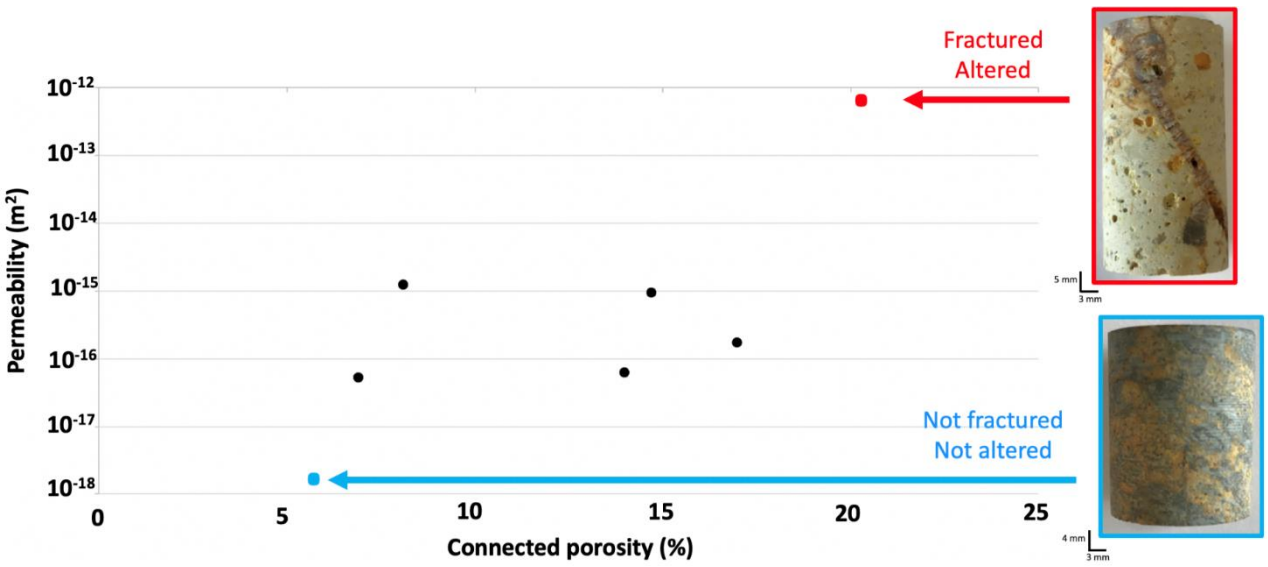

Figure 5 : Permeability and connected porosity measurements on sample taken from the Pontgibaud fault zone (Peyrouses 1 borehole). The qualitative degrees of alteration and fracturation are based on macroscopic, microscopic and three-dimensional visualization by X-ray micro-tomography observations.

4. NUMERICAL APPROACH

The numerical simulation has been performed with Comsol Multiphysics™ software. In the numerical simulations we coupled the heat transfer and fluid flow equations with appropriate rock and fluid properties. For porous and permeable formations, fluid motion is driven by the pressure gradient and buoyancy, and the fluid infiltration velocity obeys Darcy's law. Details on the used equations can be found in Guillou-Frottier et al. (2013).

In order to quantify the effect of fault zone dip and the impact of variable permeability on fluid circulation in the fault zone, a series of numerical simulations were performed. The numerical approach was organized in three successive stages. The first stage was dedicated to the study of a 2D theoretical fault zone. In order to verify the legitimacy of the digital crustal-scale model, a second stage was dedicated to the Pontgibaud hydrothermal system, in a 2D crustal-scale numerical model. The third stage consists – at present – of a preliminary study of 3D hydrothermal convection within a crustal fault zone.

Field and laboratory analyses indicate that the Pontgibaud area has a very high fracture density. By keeping the usual depth-decrease of permeability, a lateral variation can be included, by using the following spatial variation:

$$K_F(x,z) = K_{F0} \times f_{(z)} \times f_{(x)} \quad (1)$$

Where $K_F(x,z)$ is the space-dependent permeability of the fault, K_{F0} is the permeability at the surface, $f_{(z)}$ is the depth-dependent function, and $f_{(x)}$ makes the permeability alternate along a sinusoid applied to the vertical and horizontal axes of the numerical model, such as:

$$K_F(x,z) = K_{F0} \times \left[exp\frac{(-z)}{\delta}\right] \times \left[200 \times \sin\left(\frac{2\pi(z+x)}{\lambda}\right)\right] \quad (2)$$

The term λ corresponds to the wavelength of the sinusoid. To reproduce rather fine alternations of high and low permeability, as suggested by field and laboratory observations (Fig 2, Fig 3, Fig 4), a low value of λ was chosen. The length δ (m) characterizes the intensity of the decrease in permeability with depth. We can reproduce here the permeability variation corresponding to the multiple fault core conceptuel model of Faulkner et al., (2010) (Fig 7).

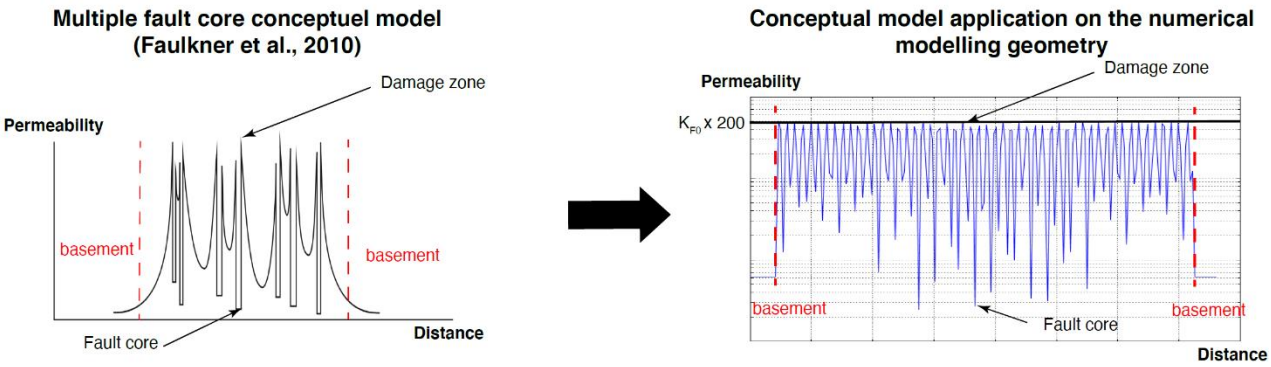

Figure 6 : Permeability imposed in the numerical models of the parametric study. The permeability of the basement and fault will decrease with depth according to equation 2. Within the fault zone, permeability will also vary lateraly, to match field observations.

4.1 Theoretical 2D fault zone

More than 200 numerical simulations have been performed. In each case, we vary the dip angle and the permeability of the fault and that's when we studies the depth and intensity of the thermal anomaly. Details on the obtained temperature patterns can be found in Duwiquet et al. (2019) and Fig 8 synthetizes all the results in graphical form. The x-axis corresponds to the dip α (°) of the structures, which vary from 20 to 160 ° from the horizontal. The y-axis corresponds to the ΔT (°C), which is the abnormal value of the temperature compared to a normal geothermal gradient and varies from 8°C to 127 °C. The different curves correspond to different permeability ratios between the fault and its host. This ratio is defined as:

$$R = \frac{K_{Fault}}{K_{Basement}} \quad (3)$$

With K_{Fault} (m^2) corresponding to the permeability of the fault, and $K_{Basement}$ (m^2) corresponding to the permeability of the basement. For a first consideration, we fixed $K_{Basement}$ at 10^{-16} m^2.

For R values between 1.9 and 39.4 (green line), dip structures have no influence on the temperature abnormally value. For R values between 59 and 137 (red line), vertical structures (~90°) concentrate the largest temperature anomalies (>110°C). For R values between 157 and 400 (blue line), the dip structures between 60 and 120 ° can have abnormal temperature values up to 80 °C.

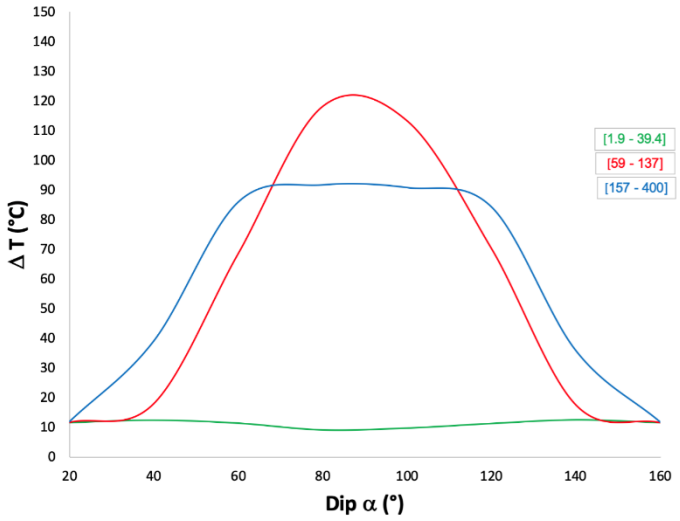

Figure 7 : Maximum of temperature anomalies as a function of the dip of the structures, and for different ranges of R values.

Figure 8 shows the range of permeability and dip for which the abnormal temperature will have a large value. However, it does not make it possible to understand how fluids circulate in a fault zone system. Fig 9 graphically summarizes the morphology of the numerically-obtained isotherms as a function of dip angle and value of thermal abnormality.

The morphology of the isotherms in the blue area (Fig 9) is slightly deformed. This low deformation occurs at dip values below 50°. The value of the resultant thermal anomaly will be lower than 65 °C. The black arrows show that the circulation of fluids is controlled by a single long-wavelength convection cell. This domain will be called the "unicellular weak type convection zone".

The morphology of the isotherms in the orange area (Fig 9) shows moderate deformation. The range of values of the thermal anomalies produced is between 10 and 120 °C. In the same way, the arrows show that fluid circulation is controlled by moderate-wavelength convection cells. This domain will be called the "unicellular medium type convection zone".

The morphology of the isotherms in the red area (Fig 9) shows significant deformation. The value of the thermal anomaly is higher than 65 °C. The black arrows show that the circulation of fluids is controlled by two short-wavelength convection cells. This domain will be called the "bicellular strong type convection zone".

This first parametric study was established in 2D and made it possible to understand the effect of permeability and dip fault on the temperature anomaly. The results of this parametric study should be applicable to hydrothermal systems in a crustal context. However,

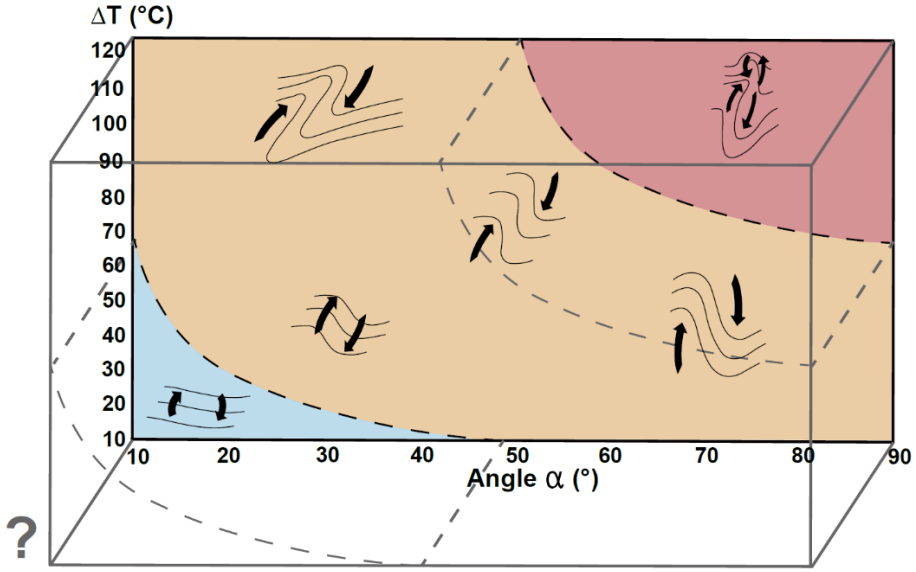

Figure 8 : Diagram of 2D convective regimes for the theoretical fault. Black curves represent isotherm morphology. The dashed black line separate three area. In blue, the area of unicellular weak type convection zone. In orange the area of unicellular medium type convection zone. In red, the area of bicellular strong type convection zone. The third variable, which may be used for 3D experiments has yet to be determined.

fluid circulation is probably dependent on the dimension (2D or 3D) in which we consider our problem. We will have to consider this question and understand the 3D effect on isotherm morphologies and the consequences on the value of temperature anomaly (the grey line in Fig 9). The regime diagram in Fig. 7 may need a third axis, which is not determined yet.

4.2 Numerical simulation of crustal-scale model and comparison with field data

The numerically-obtained heat flux and geothermal gradient are respectively 115 $mW.m^{-2}$ and 39°C/km. For this fault zone permeability, we observed the establishment of a thermal anomaly of 150°C at 2.500m (Fig 10). According to the large-scale numerical simulation and the diagram of convective regimes (Fig 9), the fluid flow circulates by bicellular strong type convection zone. Moreover, for a maximum fault zone permeability value of 1.6×10^{-14} m^2, R =160 and then confirm the quantitative approach expressed by Fig 6. However, a better understanding of the 3D spatial distribution of the 150 °C economic isotherm requires 3D numerical simulation. These 3D numerical simulations would make it possible to consider geological units not as plans but as volumes. It will then be possible to see the effects on the spatial distribution of temperature anomalies (Magri et al., 2016, Person et al., 2012, Patterson et al., 2018)

4.3 3D preliminary results

The geometry of the numerical model for Pontgibaud is directly based on the geological model and is therefore constrained by a detailed set of geological data and observations. The Pontgibaud fault zone is defined by local and regional surface heat flow values of 110 mW.m^{-2} (International Heat Flow Commission database) involving temperature gradient of 41°C/km (Fig 1). Figure 10 presents the results of the numerical simulation for a fault zone maximum permeability value of 1.6×10^{-14} m^2.

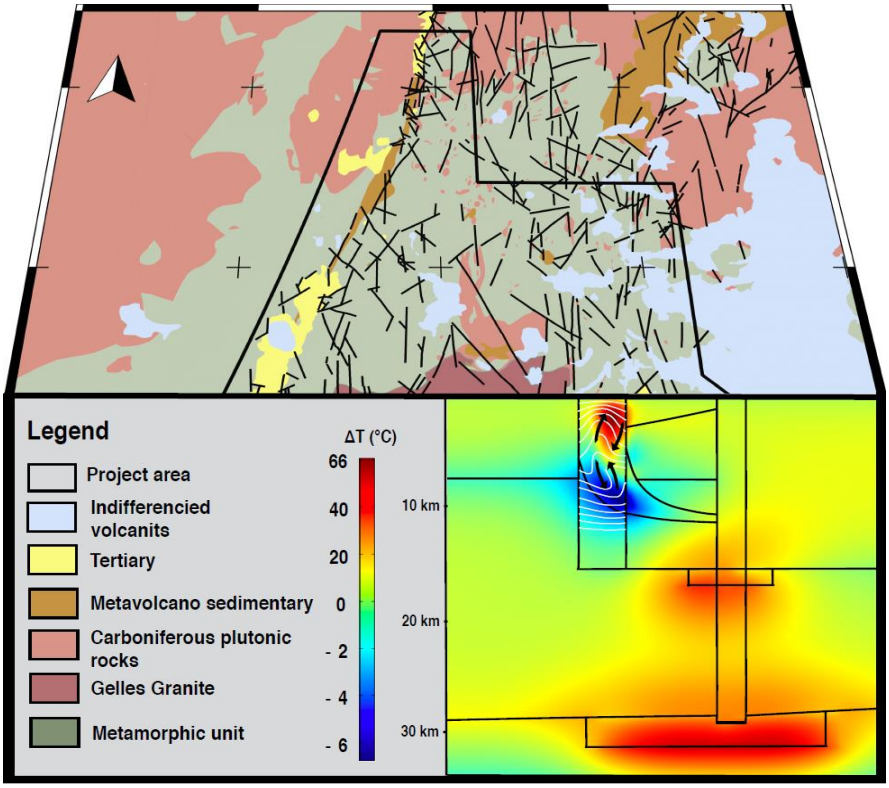

Figure 9 : Numerical simulation results for a maximum permeability value imposed on the Pontgibaud fault zone of 1.6×10^{-14} m^2. Temperature anomaly (color), isotherms in white and the circulation of fluid in black arrows. The fluid flow corresponds to a bicellular strong type convection zone.

In order to better understand the influence of the 3D space distribution on the fluid flow we first consider a simple case. The permeability of the fault is 10^{-14} m^2. The permeability of the basement is 10^{-16} m^2. Fluid circulation takes place within the fault, but also within the basement (Fig 11). Fig 11A shows that we must consider the permeability ratio between the fault and the basement. The isotherm deformation shows a depression at the extremity of both faults and an isotherm convergence in the middle of the fault. This causes a positive thermal anomaly at the middle part of the fault zone. Fig 11B shows that the envelop of the 150 °C isotherm is located at a depth between 1.500m and 5000m for a vertical structure, and thus confirm the quantitative approach expressed in Fig 6.

Other numerical simulations were performed with the same permeability values, but with a fault zone thickness of 1.0 km. Figure 12 shows that the fluid flows within the fault zone but also in the basement (Fig 12A). This is not different from Figure 11. Nevertheless, we note that the circulation patterns are different. Indeed, for a 1.0 km thickness the 150 °C anomaly is localized on the left fault zone extremity (Fig 12B). However, localization of temperature anomaly apparently depends on the thickness of the fault zone, a parameter that will be systematically studied in future simulations.

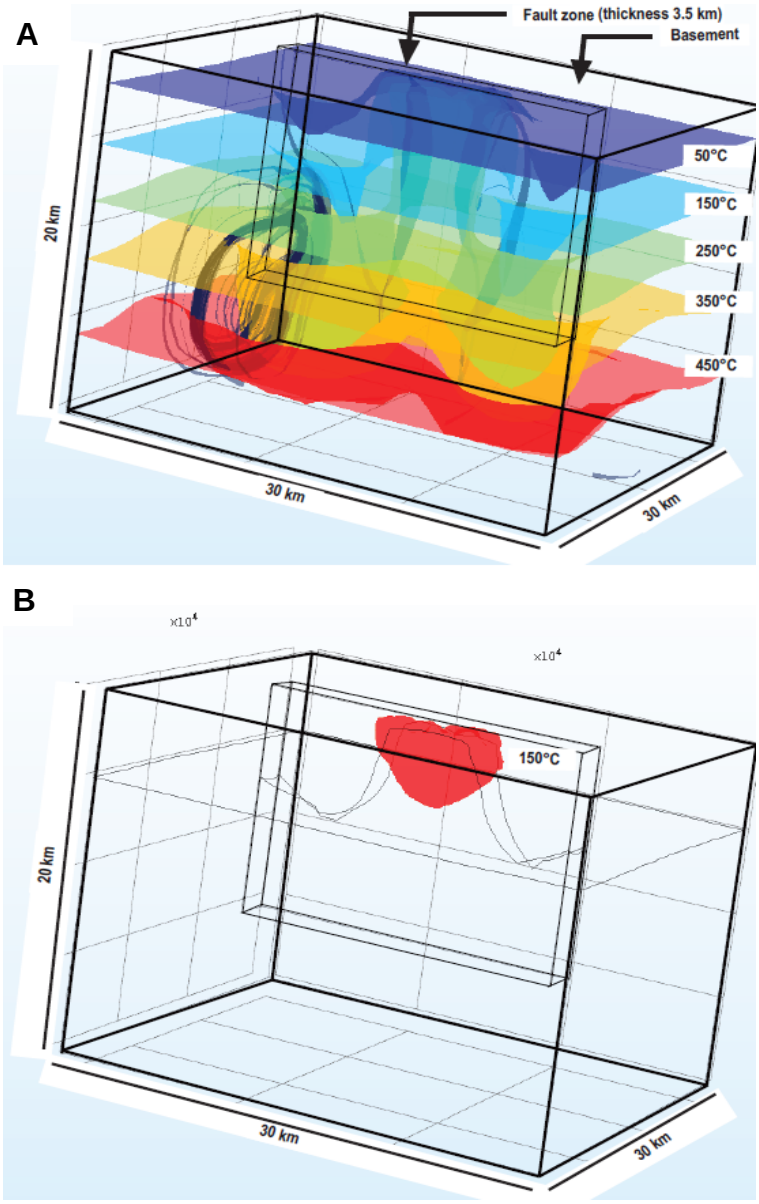

Figure 10 : (A) Dark blue, light blue, green, orange and red surfaces correspond, respectively, to 50°C, 150°C, 250°C, 350°C and 450 °C isotherms. Black lines correspond to fluid circulation streamlines (thickness of streamlines is proportional to velocity values, whose maximum is 10^{-8} m/s). (B) The red spot corresponds to the volume in which temperature exceeds 150°C (contour in thin black curves).

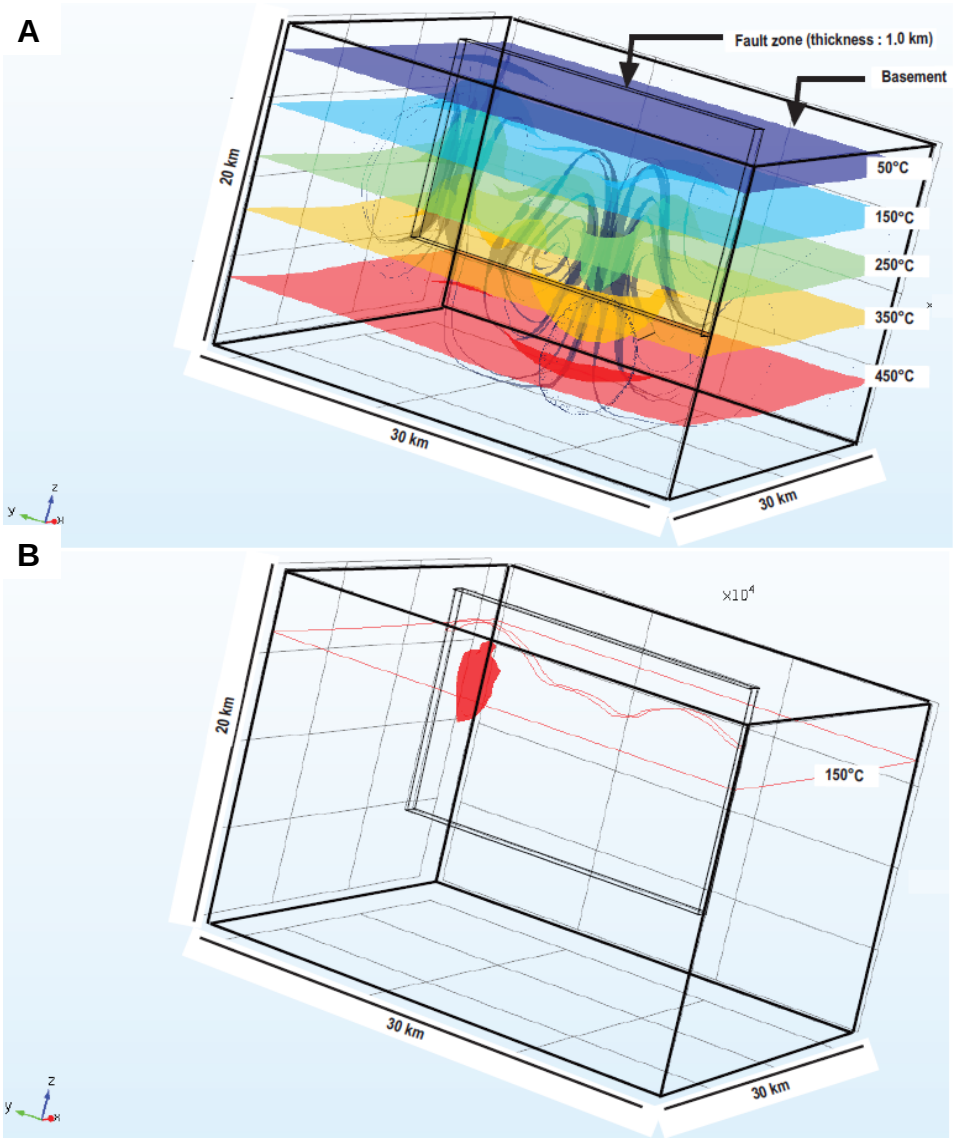

Figure 11 : (A) Dark blue, light blue, green, orange and red surfaces correspond, respectively, to 50°C, 150°C, 250°C, 350°C and 450 °C isotherms. Black lines correspond to fluid circulation streamlines (thickness of streamlines is proportional to velocity values, whose maximum is 10^{-9} m/s (B) The red spot corresponds to the volume in which temperature exceeds 150°C (contour in thin black curves).

5. CONCLUSION

This study aims to understand how crustal-scale fault zone can generate a viable geothermal resource and to better understand the organization and controlling factors of hydrothermal system associated with crustal faults. Structural observations, laboratory permeability and connected porosity measurement and X-ray micro-tomography observations suggest that the hydrothermal system have an important fracture permeability reservoir. Finally large-scale geologically constrained numerical model and its comparison with 2D parametric study and 3D preliminary results show that a temperature of 150 °C at a depth of 2500m can be obtained for a maximum Pontgibaud fault zone permeability of 1.6×10^{-14} m^2 . However, 3D preliminary results show that we must account for the geometry of the geothermal reservoir, here the Crustal Fault Zone.

REFERENCES

Ars, J. M., Tarits, P., Hautot, S., Bellanger, M., Coutant, O., & Maia, M.: Joint inversion of gravity and surface wave data constrained by magnetotelluric: Application to deep geothermal exploration of crustal fault zone in felsic basement, Geothermics, 80, (2019), 56-68. https://doi.org/10.1016/j.geothermics.2019.02.006

Bellanger, M. High temperature geothermal resources of crustal fault zones: a dedicated approach. In 79th EAGE Conference and Exhibition 2017-Workshops. (2017, June).

Brockamp, O., Schlegel, A., & Wemmer, K.: Complex hydrothermal alteration and illite K–Ar ages in Upper Visean molasse sediments and magmatic rocks of the Variscan Badenweiler-Lenzkirch suture zone, Black Forest, Germany, International Journal of Earth Sciences, *104*(3), (2015), 683-702. https://doi.org/10.1007/s00531-014-1118-2

Faulkner, D. R., Jackson, C. A. L., Lunn, R. J., Schlische, R. W., Shipton, Z. K., Wibberley, C. A. J., & Withjack, M. O.: A review of recent developments concerning the structure, mechanics and fluid flow properties of fault zones. Journal of Structural Geology, 32(11), (2010), 1557-1575. https://doi.org/10.1016/j.jsg.2010.06.009

Duwiquet, H., Arbaret, L., Bellanger, M., Guillou-Frottier, L., & Heap, M. :Are Crustal Fault Zones viable geothermal resources? Insights from the Pontgibaud Fault in French Massif Central, European Geothermal Congress (June 2019).

Famin, V., Philippot, P., Jolivet, L., & Agard, P.: Evolution of hydrothermal regime along a crustal shear zone, Tinos Island, Greece, *Tectonics*, *23*(5),(2004). https://doi.org/10.1029/2003TC001509

Guillou-Frottier, L., Carrė, C., Bourgine, B., Bouchot, V., & Genter, A.:Structure of hydrothermal convection in the Upper Rhine Graben as inferred from corrected temperature data and basin-scale numerical models, Journal of Volcanology and Geothermal Research, 256, (2013), 29-49. https://doi.org/10.1016/j.jvolgeores.2013.02.008

Heap, M. J., & Kennedy, B. M.: Exploring the scale-dependent permeability of fractured andesite, Earth and Planetary Science Letters, 447, (2016), 139-150. https://doi.org/10.1016/j.epsl.2016.05.004

Jolivet, L., Famin, V., Mehl, C., Parra, T., Aubourg, C., Hébert, R., & Philippot, P. : Strain localization during crustal-scale boudinage to form extensional metamorphic domes in the Aegean Sea, *Special papers-Geological Society of America*, (2004), 185-210.

Lahsen, A., Muñoz, N., & Parada, M. A.: Geothermal development in Chile. In Proceedings World Geothermal Congress, Bali, Indonesia. (2010, April).

Magri, F., Möller, S., Inbar, N., Möller, P., Raggad, M., Rödiger, T., ... & Siebert, C.: 2D and 3D coexisting modes of thermal convection in fractured hydrothermal systems-Implications for transboundary flow in the Lower Yarmouk Gorge, Marine and Petroleum Geology, 78, (2016), 750-758.Patterson, J. W., Driesner, T., Matthai, S., & Tomlinson, R.: Heat and fluid transport induced by convective fluid circulation within a fracture or fault, Journal of Geophysical Research: Solid Earth, 123(4), (2018), 2658-2673. https://doi.org/10.1016/j.marpetgeo.2016.10.002

Person, M., Hofstra, A., Sweetkind, D., Stone, W., Cohen, D., Gable, C. W., & Banerjee, A.: Analytical and numerical models of hydrothermal fluid flow at fault intersections, Geofluids, 12(4), (2012), 312-326. https://doi.org/10.1111/gfl.12002

Süer S, Güleç N, Mutlu H, Hilton D-R, Çifter C, Sayin, M.: Geochemical monitoring of geothermal waters (2002–2004) along the North Anatolian Fault Zone, Turkey: spatial and temporal variations and relationship to seismic activity, Pure and Applied Geophysics;165(1), (2008) 17-43. https://doi.org/10.1007/s00024-007-0294-4

Violay, M., Heap, M. J., Acosta, M., & Madonna, C.: Porosity evolution at the brittle-ductile transition in the continental crust: Implications for deep hydro-geothermal circulation, Scientific Reports, 7(1), (2017), 7705. https://doi.org/10.1038/s41598-017-08108-5